Hindawi
Geofluids
Volume 2022, Article ID 2694139, 10 pages
https://doi.org/10.1155/2022/2694139

Research Article

Numerical Test Study on the Failure Mechanism of Coal-Rock Combined Body under the Coupling Action of Hydraulic and Mechanical

Feng Chen,[1,2] **Jinguo Lv**,[2] **Yue Yin**,[2] **and Chunpeng Qi**[2]

[1]*State Key Laboratory of Coal Resources in Western China, Xi'an University of Science and Technology, Xi'an Shaanxi 710054, China*
[2]*School of Mechanics and Engineering, Liaoning Technical University, Fuxin Liaoning 123000, China*

Correspondence should be addressed to Jinguo Lv; glvjinguo2005@163.com

Received 25 October 2021; Revised 30 November 2021; Accepted 4 January 2022; Published 7 February 2022

Academic Editor: Liang Xin

Coal and rock are often in an environment of hydraulic-mechanical coupling. In order to study the failure mechanism of the coal-rock combined body under the coupling action of hydraulic and mechanical, the RFPA-Flow software was used to analyze the failure mode, strength change law, and acoustic emission change law of the coal-rock combined body with different rock-to-coal height ratios under the combined action of uniaxial load and water pressure. The research results show that the peak strength, residual strength, and stress drop of coal-rock combined body with different rock-to-coal height ratios decrease after water pressure, which reduces the occurrence probability of rock bursts. However, the stress showed a vertical drop phenomenon in the later stage of loading, indicating that the coal-rock combined body still maintains the characteristics of brittle failure after being softened by water, and the roadway may still have rock bursts. The research conclusions can provide a theoretical basis for using water injection measures to prevent rock bursts in deep coal and rock masses.

1. Introduction

The coal body does not exist alone in the stratum but exists in the form of coal and rock coexistence. The disaster accident of roadway surrounding rock is the result of the interaction between the rock body and the coal body [1–3]. If only studying the physical and mechanical properties of coal body cannot effectively guarantee the safety of coal mine production, it is necessary to focus on the physical and mechanical properties of the "roof-coal" combination coal and rock mass [4–10]. At the same time, water injection can effectively reduce the probability of rock burst occurrence in rock burst mines [11–17]. Therefore, this paper carries out a numerical experimental study on the failure mechanism of coal-rock combined body under the combined action of hydraulic and mechanical. This has important scientific significance and engineering value for the prediction and prevention of rock burst disasters in deep mines.

Many scholars have done a lot of research on the physical and mechanical properties of coal-rock combined body under different external force conditions. Gao et al. investigated the brittle failure pattern of coal–rock composite materials under uniaxial compression by laboratory tests and numerical simulations [18]. Yang et al. deduced the mathematical model of multiphysics coupling during loading and unloading of composite coal-rock [19]. Wang et al. studied the inhomogeneous characteristics of different media and the progressive failure process and acoustic emission (AE) characteristics of different coal-rock combinations [20]. Yang et al. studied the mechanical response and energy partition of coal-rock combinations with different strength ratios through laboratorial uniaxial compression tests and numerical simulation calculations [21]. Zhu et al. analyzed the mechanical properties of coal-rock combination bodies under multistage and cyclical loading–unloading [22]. Zuo et al. analyzed the postpeak progressive failure characteristics of coal-rock combined body by using the uniaxial and

triaxial compression test data [23]. Zhang et al. explored the mechanical behavior response characteristics of the combination bodies with different coal thickness proportions and analyzed the influence of the coal thickness proportion on impact failure characteristics of combination bodies [24].

The above research results pay more attention to the overall macro- and micromechanical properties and failure mechanism of coal-rock combination. However, coal and rock mass in underground engineering are often in the groundwater environment together and will be affected by the groundwater. In addition, water injection is often used in engineering to reduce the possibility of rock bursts. Therefore, taking the coal-rock combined body as the research object to carry out the related hydraulic-mechanical coupling research is closer to the actual engineering situation. Therefore, this paper uses RFPA-Flow software to study the failure mechanism of the coal-rock combined body under hydraulic-mechanical coupling. It is expected to provide a reference for the prevention and control of rock burst disasters in the process of coal resource mining.

2. Introduction to RFPA-Flow

2.1. A Brief Introduction to the Basic Principles of RFPA-Flow

(1) The seepage process in the rock satisfies the Biot consolidation theory [25].

$$\begin{aligned}
&\text{Equilibrium equation}: \frac{\partial \sigma_{ij}}{\partial x_{ij}} + \rho X_j = 0 \quad (i, j = 1, 2, 3),\\
&\text{Geometric equation}: \varepsilon_{ij} = \frac{1}{2}\left(u_{i,j} + u_{j,i}\right) \quad \varepsilon_v = \varepsilon_{11} + \varepsilon_{22} + \varepsilon_{33},\\
&\text{Constitutive equation}: \sigma_{ij} = \sigma_{ij} - \alpha p \delta_{ij} = \lambda \sigma_{ij} \varepsilon_v + 2G\varepsilon_{ij},\\
&\text{Seepage equation}: K\nabla^2 p = \frac{1}{Q}\frac{\partial p}{\partial t} - \alpha \frac{\partial \varepsilon_v}{\partial t},
\end{aligned} \tag{1}$$

where ρ is the density, σ_{ij} is the stress tensor, ε_v is the volume strain, δ is the Kronecker constant, G is the shear modulus, λ is the Lame coefficient, and ∇^2 is the Laplace operator.

(2) The relationship between permeability and stress-strain function is satisfied in the elastic state of the meso-unit, and the permeability K_f increases after the element is damaged and ruptured; the K_f can be written as

$$K_f = K_0 e^{-b\sigma'}, \tag{2}$$

where K_0 is the initial permeability coefficient, σ' is the effective stress, and b is the coupling parameter.

(3) The rock structure is nonuniform, and the damage parameters of the unit bodies composing the rock satisfy a certain probability distribution

2.2. Element Permeability-Damage Coupling Equation. When the stress state of the meso-element meets a given damage threshold, the element begins to be damaged, and the elastic modulus of the damaged element is

$$E = (1 - D)E_0, \tag{3}$$

where D is the damage variable and E and E_0 are the elastic moduli of damaged and undamaged elements, respectively.

For the element subjected to uniaxial compression, the failure criterion of the element adopts the Mohr-Coulomb criterion, namely,

$$F = \sigma_1 - \sigma_3 \frac{1 + \sin\varphi}{1 - \sin\varphi} \geq f_c, \tag{4}$$

where φ is the internal friction angle and f_c is the uniaxial compressive strength.

When the shear stress reaches the Mohr-Coulomb damage threshold, the loss variable D is expressed as follows:

$$D = \begin{cases} 0, & \varepsilon < \varepsilon_{c0}, \\ 1 - \dfrac{f_{cr}}{E_0 \varepsilon}, & \varepsilon_{c0} < \varepsilon, \end{cases} \tag{5}$$

where f_{cr} is the uniaxial compressive residual strength, ε_{c0} is the maximum compressive strain, and ε is the residual strain. It can be seen from the test that the damage will cause the permeability coefficient of the rock mass to increase sharply, and the change of the unit permeability coefficient can be described by the following formula:

$$\lambda = \begin{cases} \lambda_0 \partial^{-\beta(\sigma_1 - \partial p)}, & D = 0, \\ \xi \lambda_0 \partial^{-\beta(\sigma_1 - \partial p)}, & D > 0, \end{cases} \tag{6}$$

where λ_0 is the initial permeability coefficient; p is the pore pressure; and ξ, ∂, and β are the increase rate of the permeability coefficient, the pore pressure coefficient, and the coupling coefficient, respectively.

3. Numerical Simulation Scheme Design

The total height of the coal-rock combined body is 100 mm, among which the height of the coal body is 50, 40, 30, 20, and 10 mm; the corresponding rock body height is 50, 60, 70, 80, and 90 mm; and the coal-rock height ratio is 1 : 1, 2 : 3, 3 : 7, 1 : 4, and 1 : 9; the design scheme of the sample is shown in Figure 1. Each sample without water pressure is marked as RC50, RC60, RC70, RC80, and RC90, and each sample with water pressure is marked as SRC50, SRC60, SRC70, SRC80, and SRC90. Note: each number represents the height of the rock mass. The loading mode of the displacement control is adopted in the whole loading process, and the displacement increment Δs is 0.005 mm. At the

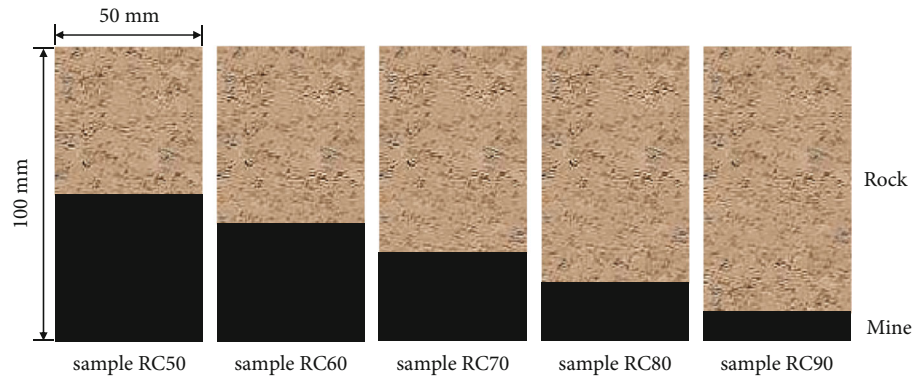

Figure 1: Schematic diagram of the design scheme of the sample.

same time, we apply a water pressure of 0.35 MPa on the lower bottom surface of the sample and 0.85 MPa on the upper top surface of the sample. The stress form of the sample is shown in Figure 2. The numerical experiment ignores the influence of the self-weight, temperature, and gas of the numerical model. The mechanical parameters of the coal and rock masses are assumed to conform to the Weibull distribution, and the failure follows the Mohr-Coulomb strength criterion. The specific coal and rock mass calculation parameters are shown in Table 1.

4. Numerical Simulation Results and Analysis

4.1. Analysis of the Failure Process of Coal-Rock Combined Body. It can be seen from Figures 3 and 4 that the cracks of samples with different coal-to-rock height ratios before and after the application of water pressure all occurred in the coal body, while the rock mass did not rupture. This is because the strength and elastic modulus of coal are less than those of rock mass, so the cracks of coal-rock combined body all occur in the coal under the action of external force. Moreover, the location of the cracks in the coal-rock combined body has nothing to do with whether the coal-rock mass is subjected to water pressure. With the decrease of coal height, the coal-rock combined body without water pressure has a different number of macroscopic cracks in the coal body; there are 3 macroscopic fracture zones in the CR50, CR60, and CR70 samples and four macroscopic fracture zones in the CR80 and CR90 samples. With the decrease of coal body height, the coal-rock combined body with hydraulic pressure has a significant difference in the fracture mode of the coal body. A macroscopic fracture zone appears in the SCR50 and SCR60 samples; not only does a macroscopic fracture zone appear in the SCR70, SCR80, and SCR90 samples but also obvious strip-shaped fracture zones appear in the coal body. The rising phenomenon indicates that the failure form of the coal-rock combined body is related to water pressure and tends to be complicated.

We take SCR70 as an example to illustrate the failure process of the coal-rock combined body after adding water pressure (see Figure 5). In the initial loading stage, the coal body has fewer failure points, is scattered, and has disorderly distribution, and no through cracks are formed in the coal

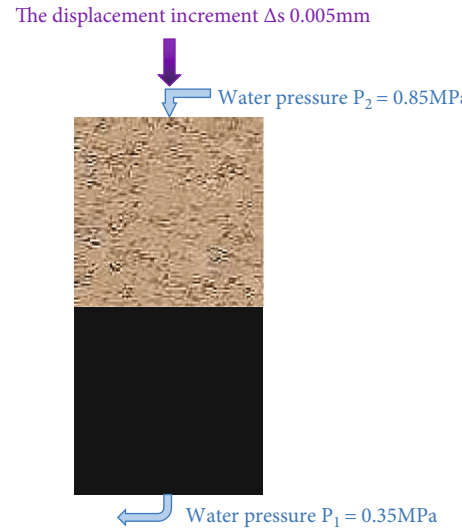

Figure 2: Method of applying external load.

Table 1: Main parameters of numerical model.

Parameter	Rock	Coal
Inhomogeneous index	5	1.5
Strength (MPa)	70.95	10.29
Young's modulus (GPa)	5.22	1.06
Poisson's ratio	0.2	0.25
Friction angle (°)	32.7	30

body. With the increase of the load, the failure points continue to increase, the phenomenon of deformation localization occurs, and some small through cracks are scattered in the coal body. With continuous loading, an obvious macroscopic crack penetrating the coal body appeared at the lower right end of the coal body. At the same time, the upper left end of the coal body was completely crushed. In the later stage of loading, the failure area at the upper left end of the coal body continues downward. Eventually, a strip-shaped failure zone appears at the left end of the coal body, and the boundary of the failure zone is very rough. With the

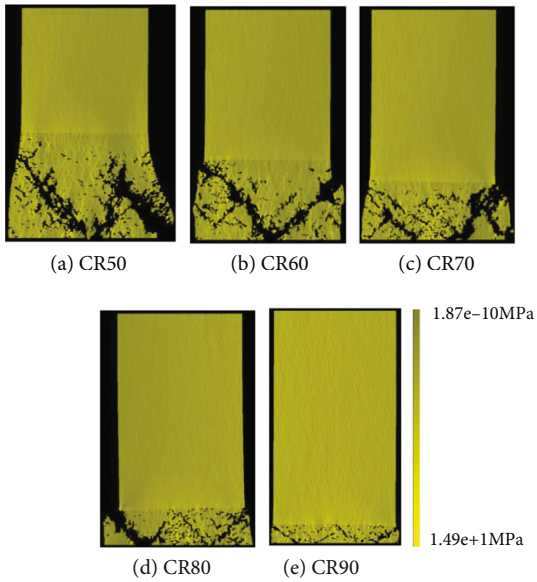

Figure 3: Fracture patterns of samples with different coal and rock height ratios without water pressure.

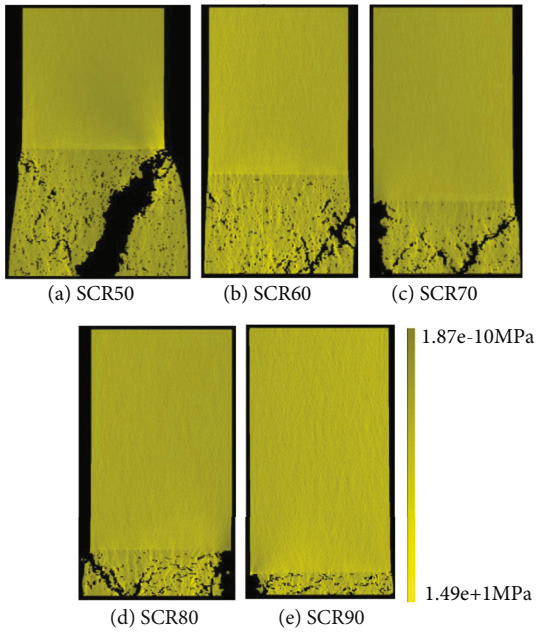

Figure 4: Fracture patterns of samples with different coal and rock height ratios after adding water pressure.

increase of the number of unit failures, the length and width of the macrocrack at the right lower end of the coal body increase, resulting in the complete separation of the right lower end of the coal body from the coal and rock mass.

4.2. Characteristic Analysis of Stress-Strain Curve of Coal-Rock Combined Body. The typical rock stress-strain curve is divided into four stages: compaction stage, elastic stage, plastic stage, and failure stage. Because the natural voids existing in the coal

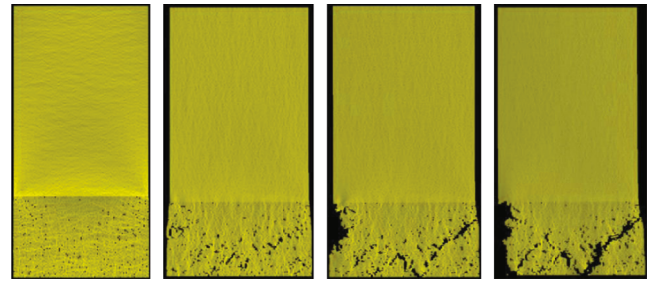

Figure 5: Fracture process of SCR70 sample.

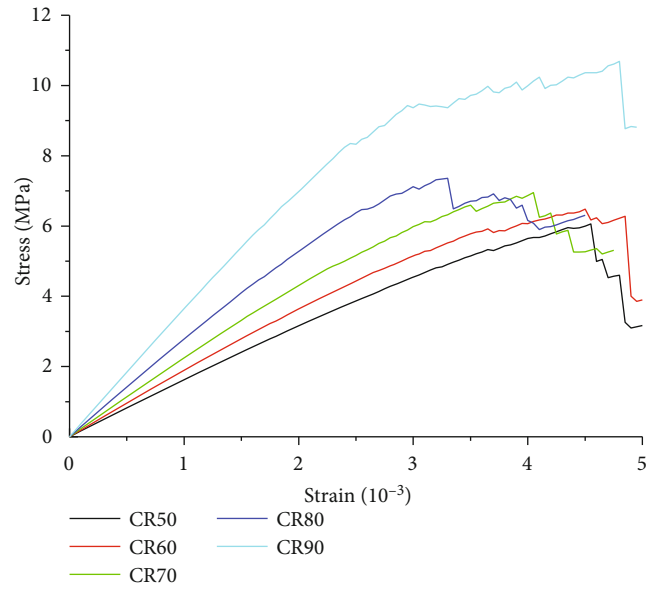

Figure 6: Stress-strain curves of samples with different coal-to-rock height ratios without water pressure.

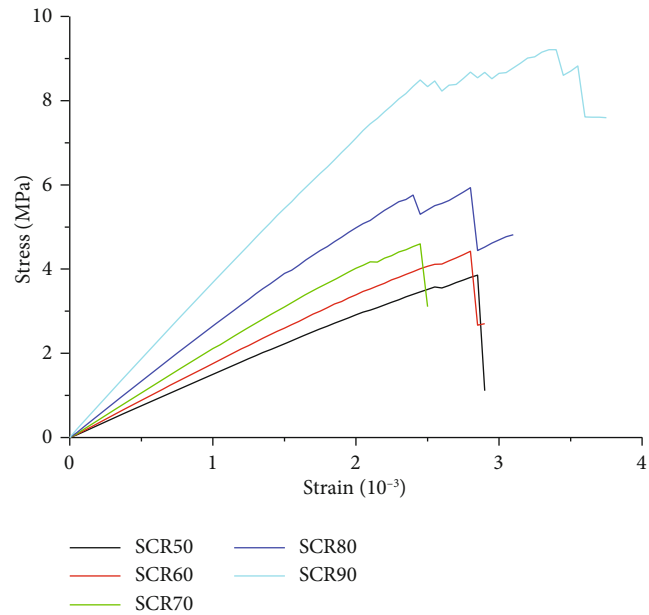

Figure 7: Stress-strain curves of samples with different coal-to-rock height ratios after adding water pressure.

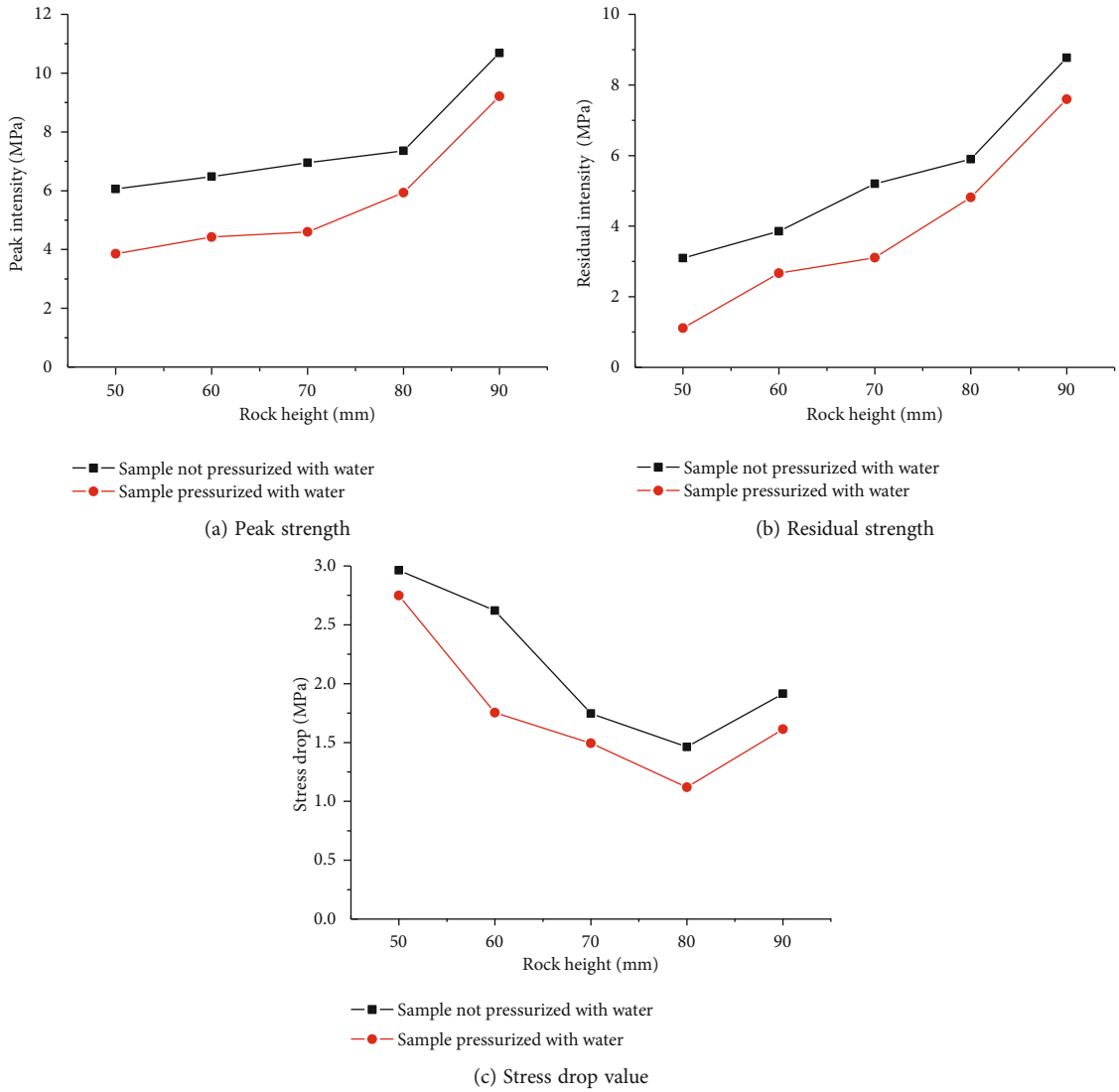

Figure 8: Strength characteristics.

and rock mass cannot be simulated in the numerical simulation, the stress-strain curve of the coal and rock mass appears in three stages during the numerical simulation: elastic stage, plastic stage, and failure stage, as shown in Figures 6 and 7. Before and after the water pressure is added, the plastic deformation stage of the coal-rock combined body increases with the decrease of coal height. Because the coal-rock combined body contains rock mass inside, when the sample fails, it has the brittle failure property when the rock mass fails. Therefore, the postpeak stage of the stress-strain curve shows a significant vertical drop.

4.3. Analysis of Strength Characteristics of Coal-Rock Combined Body. As shown in Figures 8(a) and 8(b), the peak strength and residual strength of the coal-rock combined body both increase with the increase of the rock mass height. The peak strength of coal and rock mass with water pressure is less than that of the coal-rock mass without water pressure. The reason is that the effect of pore water pressure reduces the total stress of the rock, but the deviatoric stress remains unchanged. According to Mohr-Coulomb's law, the coal-rock combined body more easily reaches peak strength. The residual strength of coal and rock mass with water pressure is less than that without water pressure. The reason is that the water molecules in the fracture weaken the cohesion between fracture particles, soften the coal and rock mass, and further reduce the mechanical properties of the coal and rock mass. The macroscopic performance is that the residual strength of the coal-rock combined body is reduced. It can be seen from Figure 8(c) that the stress drop coefficient of the coal-rock combined body first decreases and then increases. When the height of the rock mass is 80 mm, the stress drop value has a minimum value.

4.4. Analysis of Acoustic Emission Characteristics in the Damage Evolution Process of Coal-Rock Combined Body. Acoustic emission activity can directly reflect the internal damage of the loaded coal and rock mass and the initiation and propagation evolution process of microcracks. Therefore, in order to further analyze the damage evolution

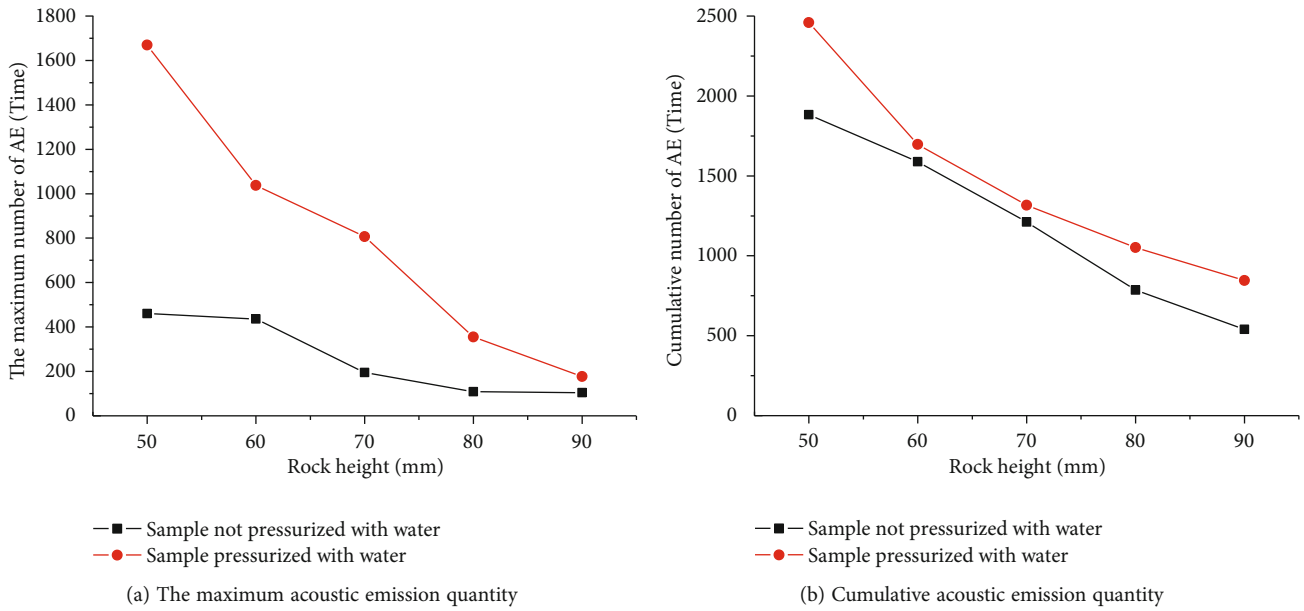

(a) The maximum acoustic emission quantity

(b) Cumulative acoustic emission quantity

Figure 9: Acoustic emission curve.

process of the coal and rock mass under hydraulic coupling, the acoustic emission quantity and cumulative acoustic emission quantity are selected as parameters to analyze the characteristics of acoustic emission in the evolution process of coal and rock mass damage under hydraulic coupling. The larger the quantity of acoustic emission and the cumulative quantity of acoustic emission, the more serious the internal damage of the coal and rock mass. It can be seen from Figure 9 that the maximum acoustic emission quantity and cumulative acoustic emission quantity decrease with the increase of rock mass height whether the coal and rock mass bears the action of water pressure or not. It shows that the quantity of acoustic emission is negatively correlated with the height of the rock mass, that is, the higher the height of the rock mass in the coal-rock combined body, the less the quantity of acoustic emission. The maximum acoustic emission quantity and cumulative acoustic emission quantity of the same coal and rock mass under water pressure are greater than those without water pressure. When the height of the rock mass is 50 mm, the maximum acoustic emission quantity of the sample pressurized with water is 3.6 times that of the sample not pressurized with water.

The time distribution characteristics of acoustic emission quantity in the whole process before and after adding water pressure to each coal and rock mass are counted. As shown in Figure 10, the acoustic emission type of the sample CR50 without water pressure belongs to the main shock-aftershock type, the acoustic emission types of CR60 and CR90 belong to the main shock type, and the acoustic emission types of CR70 and CR80 belong to the swarm type. As shown in Figure 11, the acoustic emission types of the samples SCR50, SCR60, and SCR70 with water pressure belong to the main shock type, and the acoustic emission types of SCR80 and SCR90 belong to the foreshock-main shock type.

The characteristics of each type of acoustic emission are described below. The acoustic emission characteristic of main shock-aftershock type is that the acoustic emission of the same order of magnitude occurs many times in the failure stage of the coal and rock mass. The acoustic emission characteristic of the main shock type is that the acoustic emission phenomenon mainly occurs in the coal and rock mass failure stage, and the acoustic emission quantity generated at a certain loading moment in this stage is more than 3 times or even more than 10 times that at other times. The acoustic emission characteristic of the swarm earthquake type is that the acoustic emission of the same order of magnitude is generated in each stage of coal and rock mass deformation, but the largest amount of acoustic emission occurs in the stage of coal and rock mass failure. The acoustic emission characteristic of the foreshock-main shock type is that the maximum amount of acoustic emission occurs in the failure stage of the coal and rock mass, and the same magnitude acoustic emission is also generated at a certain loading moment during the plastic deformation stage of the coal-rock mass.

4.5. Discussion. The peak strength and residual strength of the coal and rock mass decrease after adding water pressure. Moreover, there is an obvious yield stage during the loading process with the increase of the rock mass height, which reduces the excessive stress concentration and greatly reduces the probability of occurrence of rock bursts. However, the stress presents a vertical drop phenomenon, indicating that the coal-rock combined body still maintains the characteristics of brittle failure, and the roadway may still have rock bursts. This also explains why the surrounding rock mass has been softened by water injection, and rock bursts still occur.

The stress drop value of the coal and rock mass treated with water is less than that of the coal and rock mass without water, indicating that the brittleness of the coal and rock mass is significantly reduced and the

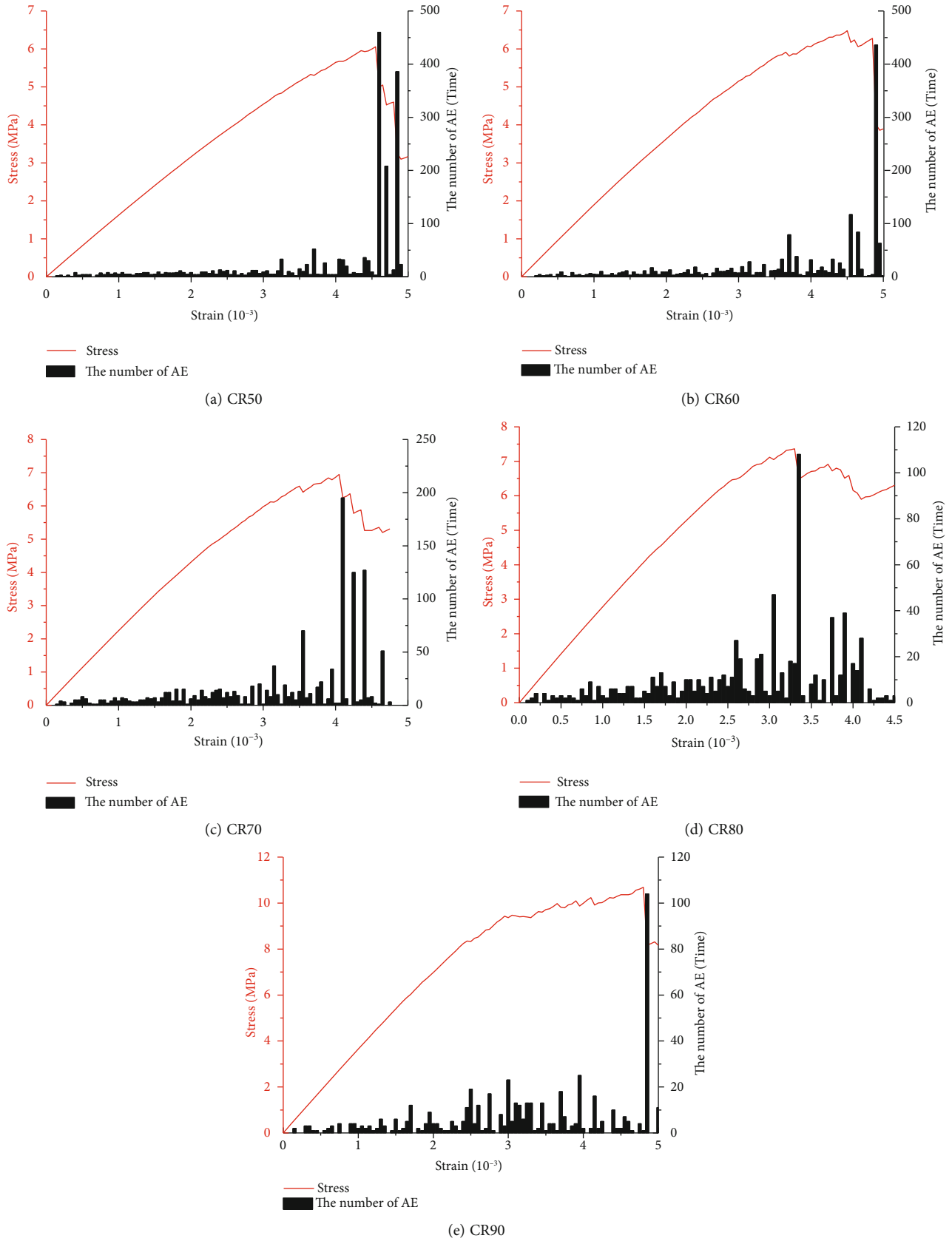

Figure 10: AE curves of samples not pressurized with water.

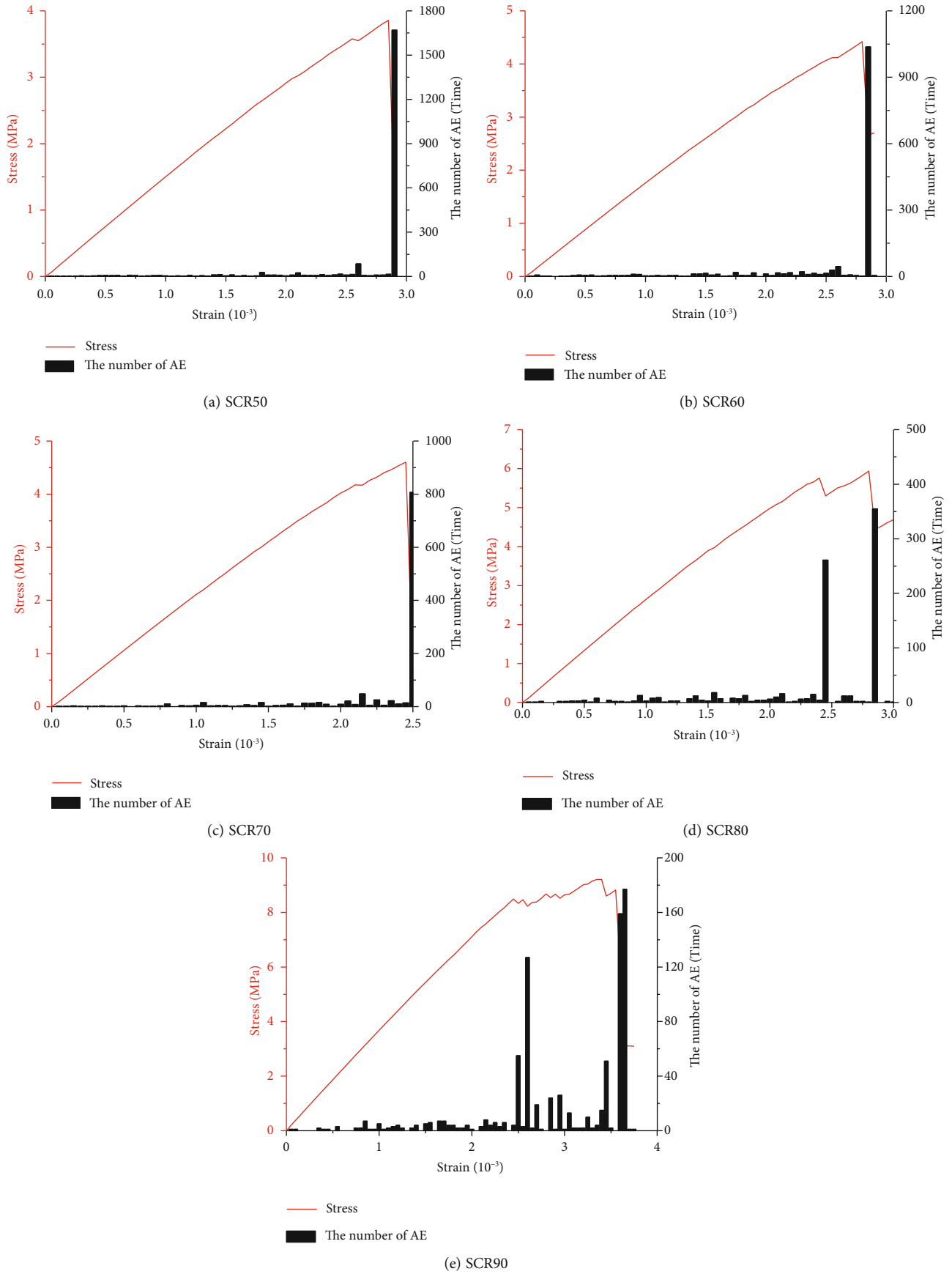

Figure 11: AE curves of samples pressurized with water.

plasticity is significantly enhanced. At the meso level, the maximum acoustic emission quantity and cumulative acoustic emission quantity fluctuate greatly, that is, the maximum acoustic emission quantity and cumulative acoustic emission quantity of the coal-rock combined body after water addition increase with the increase of coal height.

5. Conclusion

(1) Before and after the water pressure is applied, the macroscopic fracture zone of the coal-rock combined body all occurs in the coal mass, and the rock mass is not damaged. Compared with the sample not pressurized with water, the failure mode of the coal-rock combined body tends to be more complex after water pressure; not only does the macrofracture zone appear in the sample but also the obvious strip fracture zone appears in the coal body

(2) No matter whether water pressure is added or not, with the increase of rock mass height (coal height decreases), the linear elastic stage of the stress-strain curve of the coal-rock combined body decreases, and the plastic stage is more significant. For samples with the same coal-to-rock ratio, the peak strength, residual strength, and stress drop of the coal-rock combined body after adding water pressure are less than those of the coal-rock combined body without water pressure

(3) No matter whether water pressure is added or not, the acoustic emission quantity of the coal-rock combined body is positively correlated with the height of the coal body. The maximum acoustic emission quantity and cumulative acoustic emission quantity of samples with the same coal-rock height ratio under water pressure are greater than those without water pressure. The acoustic emission types of the water pressure sample are mainly the main shock type and the foreshock-main shock type

Data Availability

The data used to support the findings of this study are available from the corresponding author upon request.

Conflicts of Interest

We declare that we have no financial and personal relationships with other people or organizations that can inappropriately influence our work.

Acknowledgments

This study was supported by the State Key Laboratory of Coal Resources in Western China, Xi'an University of Science and Technology (No. SKLCRKF20-16), and the Science and Technology Research Project of the Education Department of Liaoning Province (LJ2019JL014).

References

[1] Y. Chen, J. Zuo, D. Liu, and Z. Wang, "Deformation failure characteristics of coal-rock combined body under uniaxial compression: experimental and numerical investigations," *Bulletin of Engineering Geology and the Environment*, vol. 78, no. 5, pp. 3449–3464, 2019.

[2] S. Yang, J. Wang, J. Ning, and P. Qiu, "Experimental study on mechanical properties, failure behavior and energy evolution of different coal-rock combined specimens," *Applied Sciences*, vol. 20, no. 9, pp. 4427–4444, 2019.

[3] P. Q. Qiu, J. G. Ning, J. Wang, S. C. Hu, and Z. Li, "Mitigating rock burst hazard in deep coal mines insight from dredging concentrated stress: a case study," *Tunnelling and Underground Space Technology incorporating Trenchless Technology Research*, vol. 115, article 104060, 2021.

[4] D. Malan and J. Napier, "A limit equilibrium fracture zone model to investigate seismicity in coal mines," *International Journal of Mining Science & Technology*, vol. 28, no. 5, pp. 745–753, 2018.

[5] P. Konicek and P. Waclawik, "Stress changes and seismicity monitoring of hard coal longwall mining in high rockburst risk areas," *Tunnelling and Underground Space Technology*, vol. 81, pp. 237–251, 2018.

[6] W. Y. Guo, Y. L. Tan, F. H. Yu et al., "Mechanical behavior of rock-coal-rock specimens with different coal thicknesses," *Geomechanics & Engineering*, vol. 15, no. 4, pp. 1017–1027, 2018.

[7] W. Y. Guo, T. B. Zhao, Y. L. Tan, F. H. Yu, S. C. Hu, and F. Q. Yang, "Progressive mitigation method of rock bursts under complicated geological conditions," *International Journal of Rock Mechanics and Mining Sciences*, vol. 96, pp. 11–22, 2017.

[8] F. Gao, D. Stead, and H. Kang, "Simulation of roof shear failure in coal mine roadways using an innovative UDEC trigon approach," *Computers and Geotechnics*, vol. 61, no. 3, pp. 33–41, 2014.

[9] M. He, F. Ren, and D. Liu, "Rockburst mechanism research and its control," *International Journal of Mining Science and Technology*, vol. 28, no. 5, pp. 829–837, 2018.

[10] M. C. He, H. P. Xie, S. P. Peng, and Y. D. Jiang, "Study on rock mechanics in deep mining engineering," *Chinese Journal of Rock Mechanics and Engineering*, vol. 24, no. 16, pp. 2803–2813, 2005.

[11] Z. G. Liu, A. Y. Cao, X. S. Guo, and J. X. Li, "Deep-hole water injection technology of strong impact tendency coal seam-a case study in Tangkou coal mine," *Arabian Journal of Geosciences*, vol. 11, no. 2, pp. 11-12, 2018.

[12] S. Zhu, S. Song, Q. Sun, B. Yan, and C. Wang, "Characteristics of interaction process between deep rock of lower coal seam floor and water under different test conditions," *Chinese Journal of Rock Mechanics and Engineering*, vol. 33, no. S1, pp. 3231–3237, 2014.

[13] J. He, L. Dou, S. Gong, J. Li, and Z. Ma, "Rock burst assessment and prediction by dynamic and static stress analysis based on micro-seismic monitoring," *International Journal of Rock Mechanics and Mining Sciences*, vol. 93, pp. 46–53, 2017.

[14] X. LIANG, P. HOU, Y. XUE, X. YANG, F. GAO, and J. LIU, "A fractal perspective on fracture initiation and propagation of reservoir rocks under water and nitrogen fracturing," *Fractals*, vol. 29, no. 7, article 2150189, 2021.

[15] L. Xin, Z. T. Wang, G. Wang et al., "Technological aspects for underground coal gasification in steeply inclined thin coal

seams at Zhongliangshan coal mine in China," *Fuel*, vol. 191, pp. 486–494, 2017.

[16] P. Hou, X. Liang, F. Gao, J. B. Dong, J. He, and Y. Xue, "Quantitative visualization and characteristics of gas flow in 3D pore-fracture system of tight rock based on lattice Boltzmann simulation," *Journal of Natural Gas Science and Engineering*, vol. 89, no. 4, article 103867, 15 pages, 2021.

[17] P. Hou, X. Liang, Y. Zhang, J. He, F. Gao, and J. Liu, "3D multiscale reconstruction of fractured shale and influence of fracture morphology on shale gas flow," *Natural Resources Research*, vol. 30, no. 3, pp. 2463–2481, 2021.

[18] F. Gao, H. Kang, and L. Yang, "Experimental and numerical investigations on the failure processes and mechanisms of composite coal-rock specimens," *Scientific Reports*, vol. 10, no. 1, pp. 1–13, 2020.

[19] Z. Yang, Y. Li, X. Li et al., "Multifield coupling mechanism of unloading deformation and fracture of composite coal-rock," *Shock and Vibration*, vol. 2021, no. 11, 16 pages, 2021.

[20] P. Wang, H. Jia, and P. Zheng, "Sensitivity analysis of bursting liability for different coal-rock combinations based on their inhomogeneous characteristics," *Geomatics, Natural Hazards and Risk*, vol. 11, no. 1, pp. 149–159, 2020.

[21] L. Yang, F. Q. Gao, and X. Q. Wang, "Mechanical response and energy partition evolution of coal-rock combinations with different strength ratios," *Chinese Journal of Rock Mechanics and Engineering*, vol. 39, no. S2, pp. 3297–3305, 2020.

[22] Z. H. Zhu, T. Feng, F. Q. Gong, Z. Y. Ye, and Z. Yu, "Experimental research of mechanical properties on grading cycle loading-unloading behavior of coal-rock combination bodies at different stress levels," *Journal of Central South University (Science and Technology)*, vol. 47, no. 7, pp. 2469–2475, 2016.

[23] J. P. Zuo, H. Q. Song, Y. Chen, and Y. H. Li, "Post-peak progressive failure characteristics and nonlinear model of coal-rock combined body," *Journal of China Coal Society*, vol. 43, no. 12, pp. 3265–3272, 2018.

[24] C. Y. Zhang, J. F. Pan, Y. X. Xia, and G. Y. Yang, "Research on impact failure characteristics of coal-rock combination bodies under true triaxial loading and unloading conditions," *Chinese Journal of Rock Mechanics and Engineering*, vol. 39, no. 8, pp. 1522–1533, 2020.

[25] T. H. Yang, C. A. Tang, and Q. Y. Feng, "Numerical simulation on progressive failure of loaded rock sample under pore hydraulic pressure," *Rock and Soil Mechanics*, vol. 22, no. 4, pp. 378–382, 2001, (in Chinese).